SCIENTIFIC REP⚙RTS

Self-assembly of ternary hollow microspheres with strong wideband microwave absorption and controllable microwave absorption properties

Qiang Zeng[1], Ping Chen[1], Qi Yu[2], Hai-rong Chu[1], Xu-hai Xiong[2], Dong-wei Xu[1] & Qi Wang[2]

In this study, we report a simple and efficient two-step method consisting of water-in-oil (W/O) emulsion technique and subsequent annealing process for synthesizing the hollow reduced graphene oxide microspheres embedded with Co nanoparticles (Air@rGO€Co). The microspheres showed good electromagnetic properties because of the coexistence of magnetic loss and dielectric loss to microwaves. The minimum reflection loss (RL_{min}) value of $S_{1.5}$ reaches −68.1 dB at 13.8 GHz with a thickness of 2.2 mm, and the absorption bandwidth (lower than −10 dB) is 7.1 GHz covering from 10.9 GHz to 18.0 GHz. More interestingly, we can easily control the microwave absorbing properties of the microspheres by changing the ratio of the two components in the composites. The excellent electromagnetic match at the corresponding resonance peaks for dielectric and magnetic loss play an important role in improving microwave absorption property. Our study provides a good potential method for preparation of lightweight microwave absorbing materials.

The rapid development of modern science and technology such as radar technology and modern electronic information industry has promoted increasing demand for high effective microwave absorbing (MA) materials. For example, stealth airplane, stealthy warship, and microwave darkroom[1–3]. The ideal microwave absorbing materials should possess the characteristics of thin thickness, low density, strong absorption over a broad frequency, and good chemical stability[4, 5]. Generally, basis on their microwave loss mechanism, the MA materials can be classified into two categories, including dielectric loss and magnetic loss[6]. The loss mechanism of dielectric materials such as carbon nanotubes (CNTs), graphene, carbon nanofibers (CNFs) and reduced graphene oxide (rGO) is mainly attributed to their dipolar relaxation polarization. These carbon-based materials although have some advantages such as chemical stability and light weight, but the out of balance of their dielectric permittivity and magnetic permeability will lead to most of the incident microwaves being reflected rather than absorbed[5, 7]. While the magnetic materials such as Fe_3O_4, Co_3O_4, Fe, Ni and Co although have strong magnetic loss, but the problems such as easy oxidation and high density have also hampered their applications[8].

Thus, constructing the composite absorbers with both high dielectric and magnetic loss has attracted a lot of attention, which always exhibit strong microwave absorption properties. Wang and their colleagues prepared graphene@Fe_3O_4@C@PANI composites with the mimimum reflection loss (RL) of the composites reached −44.2 dB at 11.4 GHz at the thickness of 3.0 mm[9]. Li et al. prepared SWCNT/$CoFe_2O_4$ nanocomposites with the mimimum reflection loss at 12.9 GHz and the reflection loss value of −30.7 dB at a thickness of 2.0 mm[10]. Wang et al. reported excellent MA material via an in situ oxidation polymerization of pyrrole in an aqueous dispersion of Co nanoparticles. The as-synthesized composites with a coating layer thickness of 2.0 mm exhibited a maximum absorption of −33dB at 13.6 GHz as well as a bandwidth of 4.8 GHz (at a frequency of 11.7–16.5 GHz) corresponding to reflection loss lower than −10 dB[11]. Zong et al. synthesized RGO/$CoFe_2O_4$ composites by a

[1]State Key Laboratory of Fine Chemicals, School of Chemical Engineering, Dalian University of Technology, Dalian, 116024, China. [2]Liaoning Key laboratory of advanced polymer matrix composites, Shenyang Aerospace University, Shenyang, 110136, Shenyang, China. Correspondence and requests for materials should be addressed to P.C. (email: chenping_898@126.com) or Q.Y. (email: yuqi1027@126.com)

1

one-pot hydrothermal route[12], the mimimum RL of the composite is −47.9 dB at 12.4 GHz with a thickness of 2.3 mm, and from 12.4 to 17.4 GHz the RL of the composites below −10 dB. Huang *et al*. synthesized graphene@Fe$_3$O$_4$@carbon nanocomposites, the mimimum reflection loss of the nanocomposites is −30.1 dB at 14.8 GHz with a thickness of only 1.8 mm, and the reflection loss below −10dB is ranges from 12.1 to 17.5 GHz[13]. Ren *et al*. prepared RGO–CoFe$_2$O$_4$/GNSs composites and obtained the minimum reflection loss value of −21.8 dB at 11.8 GHz with 13 wt% filler content, and the frequency bandwidth less than −10 GHz is from 9.6 to 12.4 GHz[14]. Pan *et al*. studied the microwave absorption properties of α-Co/graphene composites and β-Co/graphene composites, the results showed that the α-Co/graphene composites have excellent MA property, and the matching frequency for reflection loss exceeded −47.5 dB was at 11.9 GHz[15].

In the last few years, microcapsule techniques have gained an increasing attention due to their high potentialities in many fields, such as self-healing materials, drug delivery and anti-corrosion field. White *et al*. prepared a structural polymeric material with the ability to autonomically heal cracks[16]. The material incorporates a micro-encapsulated healing agent that is released upon crack intrusion, afte that, polymerization of the healing agent is then triggered by contact with an embedded catalyst, and bonding the crack faces. The fracture experiments yield as much as 75% recovery in toughness. Xiong *et al*. report a novel capsule-based selfrecovery system that utilizes chloride ions as a trigger[17]. Those capsules, which are functionalized via a smart response to chloride ions, are fabricated using a silver alginate hydrogel that disintegrates upon contact with chloride ions, and thereby releases the activated core materials which can be precipitated with chloride ions. They introduce the capsules into cementitious materials, and prove the capsules still can be responsive to chloride ions in concrete matrix. Therefore, the capsules will be a promising candidate for building materials and prolong the life of construction and building materials, especially in marine environment. Wang *et al*. fabricated a self-immunity microcapsule which can be triggered by low pH values, and calcium hydroxide can be controllably released to regulate the environmental pH condition and decrease the [Cl$^-$]/[OH$^-$] ratio, reach corrosion protection of steel bar in reinforced concrete. Furthermore, test results show that the release rate of core materials could interact with environmental pH value; the rate increases markedly with decreasing pH value, but is inhibited by high pH values[18]. Cui *et al*. fabricated multi-stimuli responsive smart chitosan-based microcapsules (MSRS-CS-MCs) via a facile sonochemical method[19]. The obtained spherical MSRS-CS-MCs with the average size of 500 nm showed excellent magnetic responsive ability, favorable selectively folate-receptor-mediated targeting functionality to the HeLa cells, and attractive reduction-responsive release ability for hydrophobic drugs, which make MSRS-CS-MCs promising nanocarriers for future biomedical applications.

MA performances of microwave absorbing materials are closely related to their microstructures[20, 21]. In order to improve the dielectric-magnetic composite MA performance further, many efforts have been devoted to developing novel MA absorber with special structures, such as barium ferrite@poly (3,4-ethylenedioxy thiophene), Fe$_3$O$_4$@TiO$_2$, Fe$_3$O$_4$@ZnO, Ni@P, CoNi@SiO$_2$@TiO$_2$, CoNi@Air@TiO$_2$[1, 22–27]. These core/shell or Yolk/shell multicomponent hierarchical microspheres with magnetic/dielectric absorption components, can generate tunable reflection loss by changing the type and relative content of core/shell component, thereby improving the impedance matching in terms of complex permittivity and permeability. Typically, based on our previous works, it confirms that hollow hybrid 3D microspheres have excellent MA performance[28].

Herein, we report a facile and efficient procedure for preparation of hollow hybrid 3D microspheres (Air@rGO€Co microspheres), in which Co nanoparticles were embedded within the spongy shell assembled by rGO nanosheets. These Air@rGO€Co microspheres show strong wide band and controllable microwave absorption properties. The minimum reflection loss (RL$_{min}$) value of S$_{1.5}$ reaches −68.1 dB at 13.8 GHz with a thickness of 2.2 mm, and the absorption bandwidth (lower than −10 dB) is 7.1 GHz covering from 10.9 GHz to 18.0 GHz. The excellent absorption capability could be attributed to the special 3D morphology with hollow cavities, the intrinsic magnetic loss from Co nanoparticles and dielectric polarization loss from the rGO nanosheets. Interestingly, we can easily controll the microwave absorbing properties of the microspheres by changing the ratio of the two components in the composites.

Experimental section

Materials.
All chemical regents including concentrated hydrochloric acid (HCl), polyvinyl alcohol, ethyl alcohol and acetylacetone cobalt(II)(AACo) were purchased from Sinopharm Chemical Reagent Co., Ltd (Shanghai, China). Olive oil (Olivoilà) and deionized water obtained from a Milli-Q system (Millipore, Bedford, MA) were used.

Preparation of GO aqueous dispersion.
GO was synthesized from natural graphite powder using a modified Hummers method[28]. The resulting solid GO were dispersed in water under ultrasound treatment to obtain an aqueous dispersion of GO nanosheets (4.5 mg ml^{-1}).

Synthesis of the Air@rGO€Co microsphere.
Polyvinyl alcohol (PVA, 0.3 g), acetylacetone cobalt (AACo, 1.5 g) and absolute ethyl alcohol (50 ml) were mixed with GO suspension (4.5 mg ml^{-1}, 20 ml) and stirred for several hours to obtain homogeneous suspension. The obtained suspension was then slowly added into the hot olive oil (preheated to 75 °C) under intense stirring (6000 r min^{-1}) to form stable water-in-oil emulsions. The emulsion system was kept stirring with speed of ~500 r min^{-1} for two hours at 75 °C to remove the ethyl alcohol, followed by heated to 95 °C with continuously stirring for another two hours to remove the water and the remaining ethyl alcohol. Finally, the emulsion system was cooled down to room temperature and the GO/AACo/PVA microspheres were separated and purified by centrifugation, washing and drying. The obtained microspheres precursor was calcined at 550 °C in Ar atmosphere for two hours to obtain the Air@rGO€Co microspheres and labeled as S$_{1.5}$. The schematic illustration for the self-assembly process of Air@rGO€Co microspheres is shown in Fig. 1. For comparison, GO/AACo/PVA microspheres with different amounts of AACo (0, 0.5, 1.0, 2.0, and
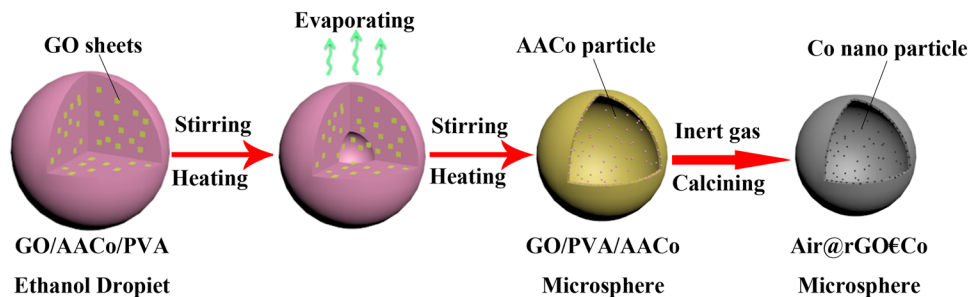
Figure 1. A schematic illustration for the self-assembly process of Air@rGO€Co microspheres.
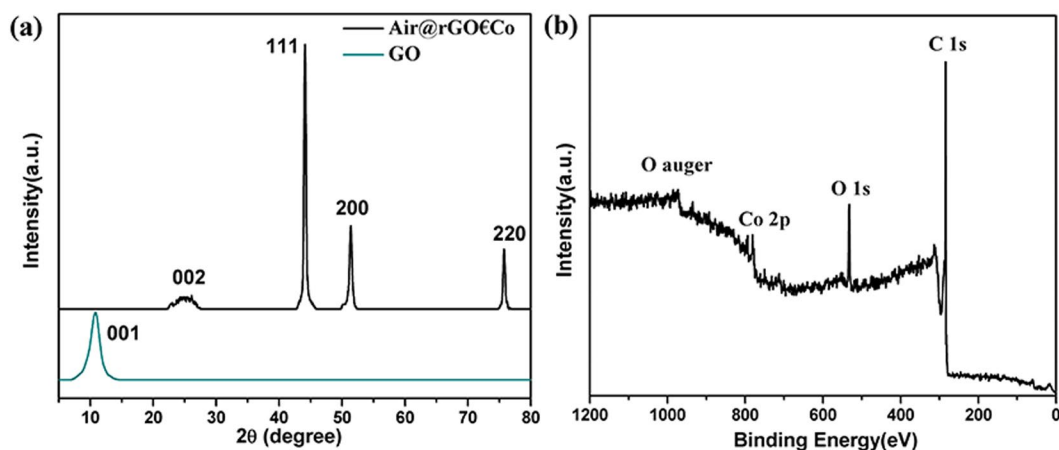

Figure 2. (**a**) XRD patterns of $S_{1.5}$ (**b**) The XPS full spectrun of $S_{1.5}$.

2.5 g) were addedthe, and the corresponding Air@rGO€Co microspheres were labeled as S_0, $S_{0.5}$, $S_{1.0}$, $S_{2.0}$ and $S_{2.5}$, respectively. Pure Co nanoparticles were prepared by calcining AACo in the same conditions and labeled as S_p.

Characterization. The composition and phase purity of the as-synthesized samples were analyzed by X-ray diffraction (XRD) with monochromatized Cu-Kα incident radiation by a Rigaku D/Max-2400 instrument operating at 12 kV voltage. The size and morphology of the samples were characterized by a Hitachi Su3500 scanning electron microscope (SEM) equipped with an energy dispersive spectrometer (XFlash 5030, Bruker, Germany), along with a field–emission transmission electron microscope (TEM, Tecnai F30, USA). AFM analysis was conducted on a PicoScanTM 2500(USA). X-ray photoelectron spectroscopy (XPS) was recorded on an ESCALAB 250 spectrometer (Thermo Fisher) to characterize the surface composition. The complex permittivity and permeability were measured using the waveguide technique at the frequency range of 1−18 GHz with an Agilent 8720ET network analyzer. These products were uniformly blended with paraffin matrix with a mass ratio of 1:2, and the mixture was cast into a ring mold with thickness of 2.0 mm, inner diameter of 3 mm, and outer diameter of 7 mm.

Results and Discussion

The synthesis process of Air@rGO€Co microsphere is depicted in Fig. 1, where PVA acts as the binder between AACo particles and GO nanosheets as well as the framework of microsphere, which can be ablated off after calcination in Ar atmosphere. In the calcination process, GO nanosheets which have been reduced to rGO were linked together by the reactions of rested hydroxy, epoxy and carboxy group. Simultaneously, PVA was pyrolyzed and AACo particles were calcined to be Co nanoparticles at high temperature. The crystallinity of the nanoparticles was characterized by X-ray diffraction (XRD). As seen from Fig. 2a, all diffraction peaks can be assigned to the (111), (200) and (220) lattice planes of the cubic spinel structured Co (JCPDS No.15–0806). The appearance of diffraction hump (002), which originates from the short-range order of stacked graphene sheets, and the disappearance of diffraction peak (001) confirm that the GO sheets were completely reduced in the calcination process[29, 30]. The chemical composition of $S_{1.5}$ was studied by X-ray photoelectron spectroscopy (XPS). The peaks associated with C 1 s, O 1 s, and Co2p indicate that the microsphere consists of three elements including C, O and Co (Fig. 2b).

Figure 3a,b show a representative scanning electron microscopy (SEM) images of the Air@rGO€Co microspheres ($S_{1.5}$), which show hollow spherical structure. The size of microspheres is not uniform and their diameters are normally distributed, and the size distribution analysis of Air@rGO€Co microspheres was shown in Fig. S1 (Supplementary information). The result shows that the range of microspheres diameters is 3 to 6 μm, and the
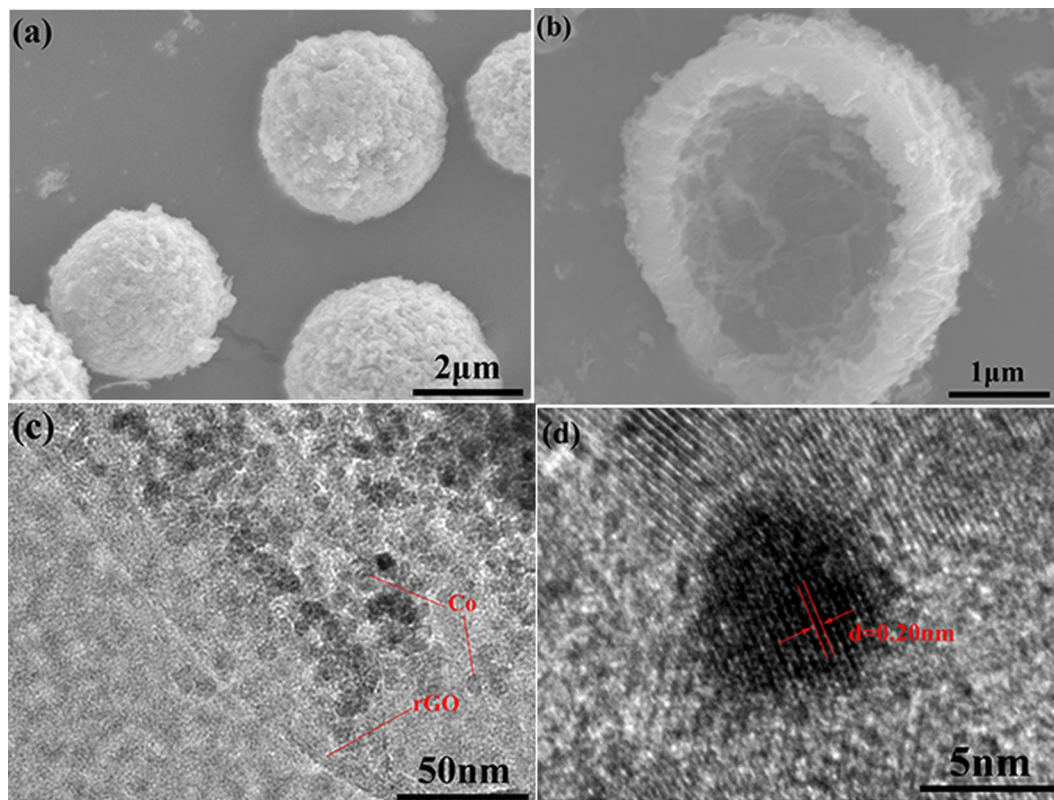
Figure 3. SEM images of (**a**) Air@rGO€Co microspheres (S$_{1.5}$), (**b**) cross-section of microsphere. (**c**) TEM image of a fragment from a microsphere which has been ultrasonic decomposed, (**d**) high magnification TEM image of the fragment.

mean diameter is 4.2 μm. There presents a hollow-core construction in the interior of the microspheres and the thickness of the spongy shell is about 0.5 μm (Fig. 3b). Transmission electron microscopy (TEM) images in Fig. 3c show that Co nanoparticles are sandwiched between the rGO nanosheets with an average size of 7 nm. Moreover, the high-resolution image (as shown in Fig. 3d) revealed a distance between atoms of *ca*. 0.20 nm, which corresponds to the distance between the (111) planes of Co. The energy disperse spectroscopy (EDS) elemental mappings (Fig. S2d–f, Supplementary information) show different distribution patterns for C, O and Co elements. The EDS line scanning analyses (Fig. S2c, Supplementary information) reveal that the relative concentration of Co element increases from outer to inner surface of the microsphere wall, which will be benefit to improve the corrosion resistance of the Air@rGO€Co microspheres.

The electromagnetic properties (complex permittivity and permeability) of Air@rGO€Co microspheres were investigated in the frequency range of 1.0−18.0 GHz at room temperature. The real permittivity (ε') and real permeability (μ') represent the storage ability for electromagnetic energy, and the imaginary permittivity (ε'') and imaginary permeability (μ'') are an expression for the dissipation of energy and magnetic loss, respectively[31]. The dielectric loss tangent ($tan\,\delta\varepsilon = \varepsilon''/\varepsilon'$) and the magnetic loss tangent ($tan\,\delta\mu = \mu''/\mu'$) are used to describe the corresponding dielectric and magnetic loss ability[32, 33].

The samples used for the measurement of electromagnetic properties were prepared by mixing the paraffin wax and Air@rGO€Co microspheres (mass ratio was 2:1). As shown in Fig. 4a, the real part of permittivity (ε') value of S$_{1.5}$ is located within the range of 6–12, and the imaginary part of permittivity (ε'') value is located within the range of 3.1–4.3. The parameters of the relative complex permeability for the sample is shown in Fig. 4b, the real part of permeability (μ') values display a decrease trend with the increase of frequency, and the imaginary part of permeability (μ'') value is within the range of 0.15−−0.17.

The dielectric loss tangent and the magnetic loss tangent are shown in Fig. 4c. The presence of multiple loss peaks on the dielectric loss tangent curve suggests complex dissipation mechanisms of dielectric loss process. Multiple polarization processes may cause these resonance peaks, including the interface polarization induced by the presence interface between the Co and rGO[34], and the polarization of existing defects and functional groups in the rGO[35]. Multi-resonance peaks which are induced by multiple magnetic loss mechanisms can be observed at 2–16.5 GHz in the magnetic loss tangent curves[36, 37]. The peaks detected at the low-frequency range of 2–6 GHz are related to natural resonance[38], and the resonance peaks appearing in the middle-frequency (6–12 GHz) are ascribed to the dipolar polarization and exchange resonances[36, 39, 40]. According to the Maxwell equations, a magnetic field can be induced by an *ac* electric field and the magnetic energy can transferred into the electric energy[41]. Thus, the magnetic loss tangent and increased dielectric loss tangent value of Air@rGO€Co microspheres in
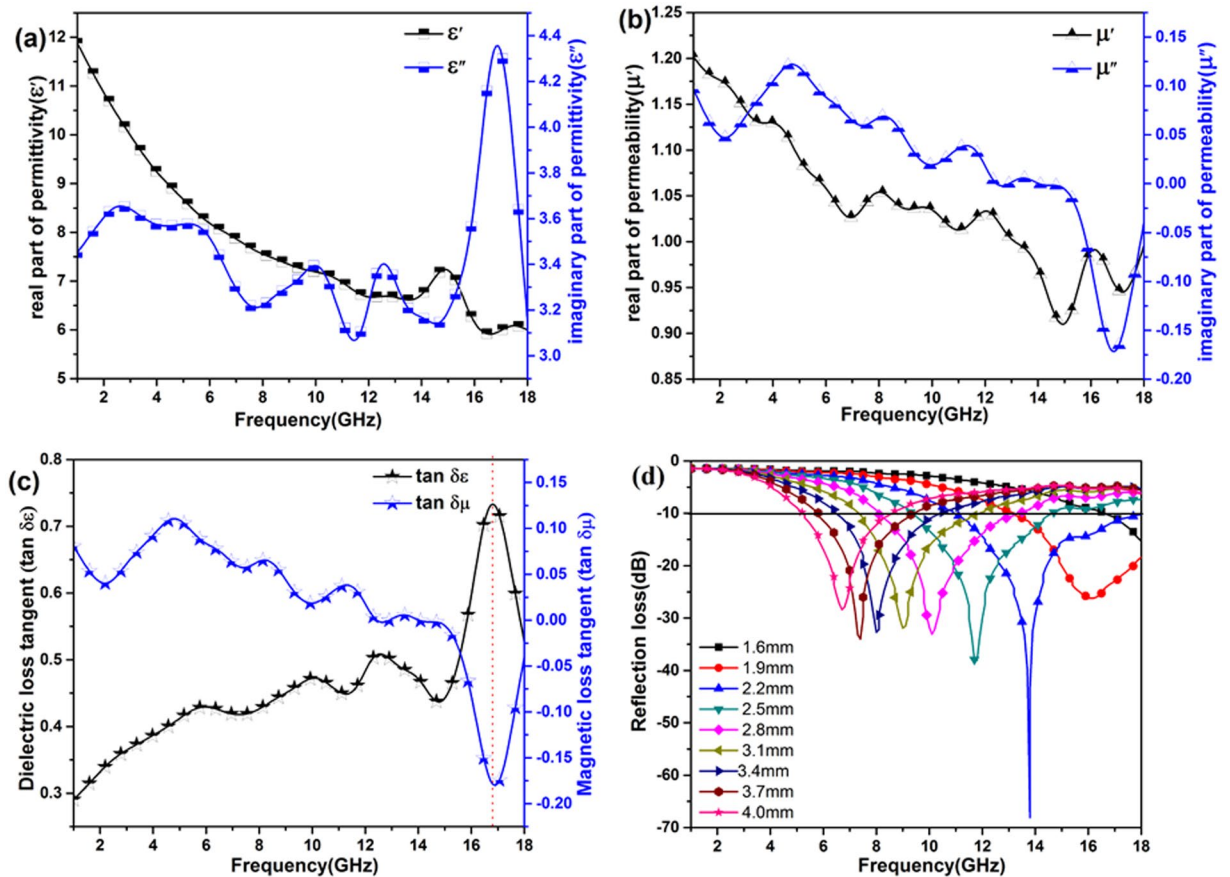
Figure 4. Relative complex permittivity (**a**), relative complex permeability (**b**), dielectric loss tangent (tan δ_ε) and magnetic loss tangent (tan δ_μ) (**c**) of paraffin composites filled with 33.3 wt% $S_{1.5}$, and the calculated reflection loss of paraffin composites with different thicknesses (**d**).

the frequency range of 15.0–18.0 GHz (Fig. 4c) denotes that the magnetic energy is transferred into the electric energy.

Based on above EM parameters, the reflection loss (RL) was calculated based on the relative complex permittivity and permeability at a given frequency and thickness according to the following equations[3, 38]:

$$Z_{in} = \sqrt{\mu_r/\varepsilon_r}\,tanh\left[-j(2\pi fd/c)\sqrt{\mu_r/\varepsilon_r}\right] \tag{1}$$

$$RL(dB) = 20\log_{10}\left|(Z_{in} - 1)/(Z_{in} + 1)\right| \tag{2}$$

where ε_r and μ_r are the relative complex permittivity ($\varepsilon_r = \varepsilon' - j\varepsilon''$) and permeability ($\mu_r = \mu' - j\mu''$) of the absorber, f is the frequency of microwave in free space, c is the velocity of light, d is the coating thickness and Z_{in} is the input impedance of the absorber. When the RL valve is lower than -10 dB, it means that only 10% of the incident microwave is reflected while 90% of the microwave is absorbed. Conventionally, we define the frequency range over which the RL value lower than -10 dB as the effective absorption bandwidth. Figure 4d shows the calculated RL of paraffin/$S_{1.5}$ (mass ratio was 2:1) composites at different thicknesses (1.6–4.0 mm). The minimum reflection loss (RL_{min}) value of the composites reaches -68.1 dB at 13.8 GHz (matching thickness is 2.2 mm), and the absorption bandwidth (lower than -10 dB) is 7.1 GHz covering from 10.9 GHz to 18.0 GHz. Otherwise, Fig. 4d presents an interesting phenomenon, as the matching thickness increased the reflection loss peak moved to a lower frequency region. The 1/4 wavelength equation can be used to explain above mentioned law[42]:

$$t_m = nc/4f_m(\mu_r\varepsilon_r)^{1/2} \tag{3}$$

where t_m is matching thickness, f_m is the frequency of the RL_{min} peaks, ε_r and μ_r are the complex permittivity and permeability, respectively, at the f_m, and c is the velocity of light.

Electromagnetic parameter is the key factor in improving the absorbing performance of the composites. Changing the ratio between AACo and the GO will obtained Air@rGO€Co microspheres with different electromagnetic parameter. In this way, the adjustable MA property of the composites can be realized. The electromagnetic parameters of S_0, $S_{0.5}$, $S_{1.0}$, $S_{2.0}$, $S_{2.5}$ and S_P were shown in Figs S3–S8 (Supplementary information),
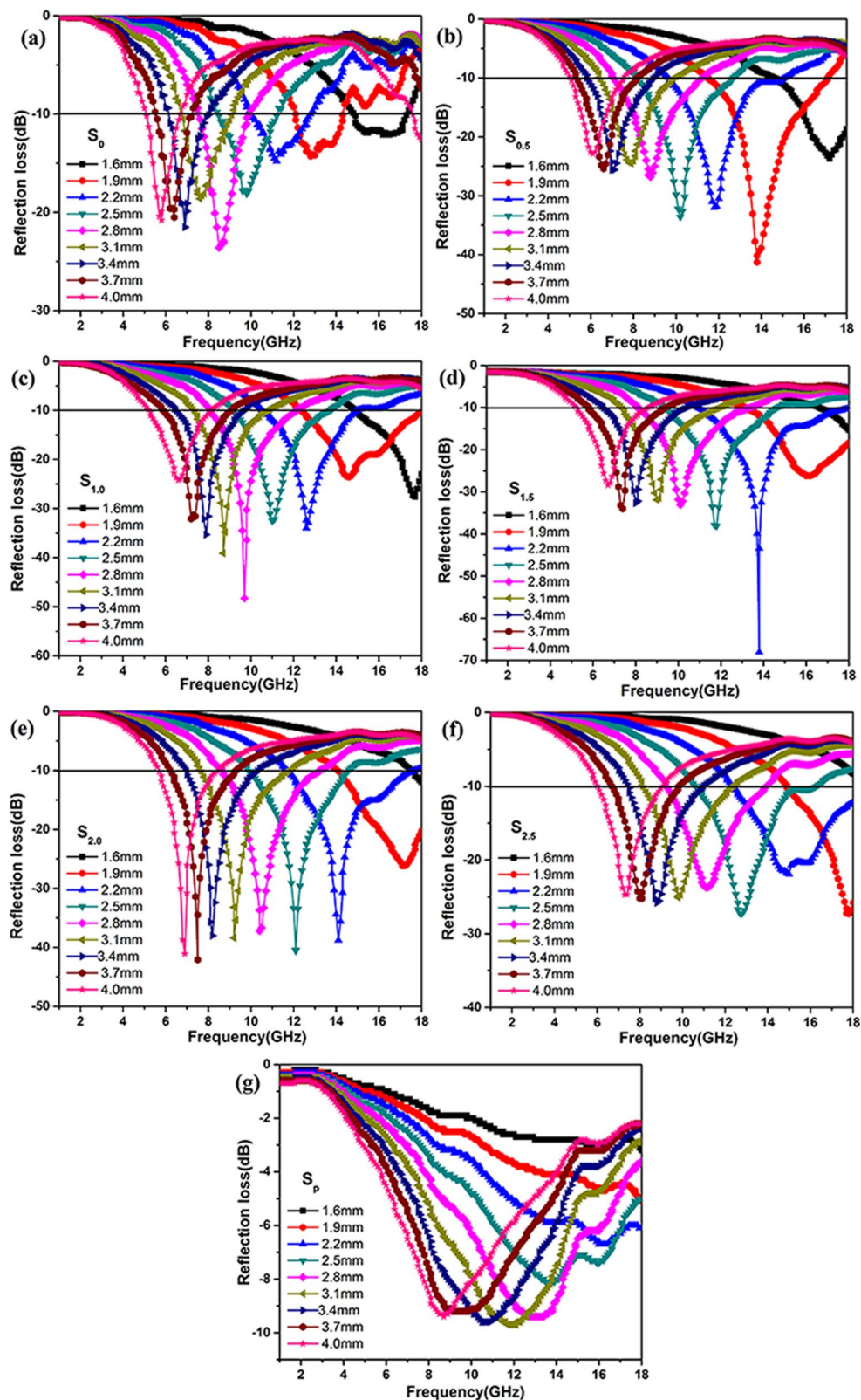
Figure 5. Calculated reflection loss of (**a**) S_0, (**b**) $S_{0.5}$, (**c**) $S_{1.0}$, (**d**) $S_{1.5}$, (**e**) $S_{2.0}$, (**f**) $S_{2.5}$, (**g**) S_p with differents thickness in the frequency range of 1–18 GHz.

and the reflection losses were calculated based on the electromagnetic parameters. As indicated in Fig. 5b–f, the Air@rGO€Co microspheres with different Co contents were also exhibit excellent microwave absorption ability. Comparing with the sample shown in Fig. 5a–g, it can be found that as the AACo content increase, the RL_{min} valve

Samples	RL$_{min}$ [dB]	The frequency of RL$_{min}$ [GHz]	Frequency range [GHz] (RL $\leq$ −10 dB)
S$_0$	−14.8	11.2	10.0–12.7
S$_{0.5}$	−32	11.8	9.7–15.1
S$_{1.0}$	−34	12.6	10.6–14.9
S$_{1.5}$	−68.1	13.8	10.9–18.0
S$_{2.0}$	−38.1	14.1	11.7–17.7
S$_{2.5}$	−21.1	15.0	12.4–18.0
S$_p$	−6.7	16.4	—

Table 1. The minimum reflection loss value (RL$_{min}$), the frequency of RL$_{min}$ and the absorption bandwidth of differents samples under the thickness of 2.2 mm.
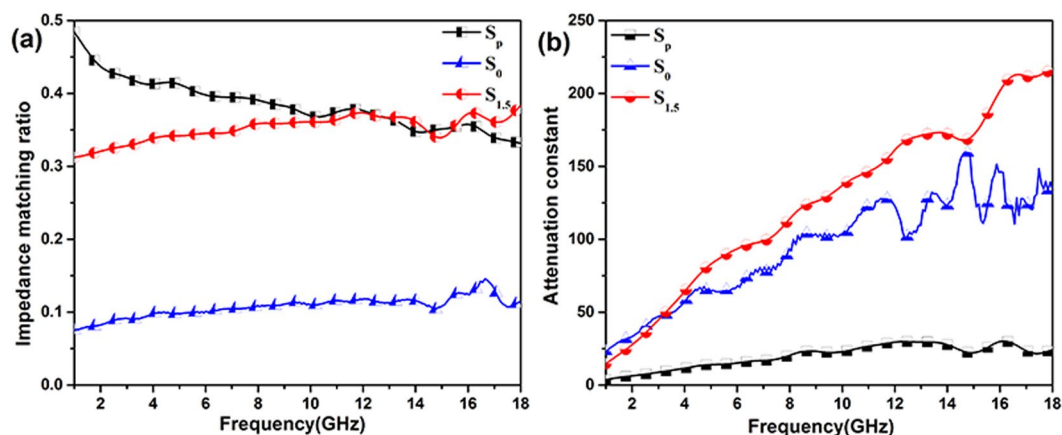
Figure 6. (**a**) Impedance matching ratio Z, (**b**) attenuation constant α of S$_p$, S$_0$ and S$_{1.5}$.

of Air@rGO€Co microspheres move to higher frequency range. The minimum reflection loss value (RL$_{min}$), the frequency of RL$_{min}$ value and the absorption bandwidth of differents samples under the thickness of 2.2 mm were shown in Table 1.

The increasing content of AACo will introduce more magnetic component of Co nanoparticles into the microspheres. As shown in Figs S3–S8 (Supplementary information), the permeability of Air@rGO€Co microspheres increase with the increasing Co contents, thus results in the enhanced magnetic loss. The primary magnetic loss mechanism of Co nanoparticles is exchange resonance in higher frequency range[11], so the microsphere with more Co content has a better absorption of microwave in higher frequency range. Meanwhile, the increasing content of Co means the density of rGO in the microspheres was decreased. On the contrary, the permittivity of Air@rGO€Co microspheres decrease with the increasing Co contents (Figs S3–S8, Supplementary information), meaning that the dielectric loss was weakened. Debye dipolar relaxation is main dielectric loss mechanism of rGO in lower frequency domain[28], so the microsphere with more rGO content has a better absorption of microwave in lower frequency range.

As a result, we can easily controll the microwave absorbing frequency range and RL valve of the microspheres by changing the ratio of the two components in the Air@rGO€Co microspheres.

From Fig. 5a,d and g, the minimum reflection loss value of S$_0$ and S$_p$ was no more than −25 dB, while that of S$_{1.5}$ at a coating thickness of 2.2 mm was as much as -68.1 dB. The Air@rGO€Co microspheres which composed of dielectric loss material (rGO) and magnetic loss material (Co) exhibit strong microwave absorption properties. To evaluate the MA performance of material, impedance matching Z and attenuation constant α are two of the most important parameters, as expressed by the following equation[43]:

$$Z = \sqrt{\sqrt{(\mu'^2 + \mu''^2)}/\sqrt{(\varepsilon'^1 + \varepsilon''^2)}} \tag{4}$$

$$\alpha = \frac{\sqrt{2}\,\pi f}{c} \times \sqrt{(\mu''\varepsilon'' - \mu'\varepsilon') + \sqrt{(\mu''\varepsilon'' - \mu'\varepsilon')^2 + (\mu'\varepsilon'' - \mu''\varepsilon')^2}} \tag{5}$$

where f is the frequency of the microwave and c is the velocity of light. Good impedance matching behavior of an absorbent means that most of incident electromagnetic wave can enter into material interior and be attenuated, rather than being reflected on the material surface. It is observed from Fig. 6a that the S$_0$ have the lowest impedance matching ratio value, while the S$_p$ have the highest impedance matching ratio value but the lowest attenuation constant α (Fig. 6b). As a consequence, both the S$_0$ and the S$_p$ show relatively poor microwave absorption

properties. In contrast, the $S_{1.5}$ have a moderate impedance matching ratiowhich is lower than that of S_p and higher than that of S_0 (Fig. 6a), and fascinating attenuation ability according to Fig. 6b. Their attenuation values are much higher than that of the S_p and the S_0 over 1–18 GHz. Overall, the $S_{1.5}$ which could effectively offset the drawbacks of the sole Co nanoparticles or rGO nanosheets, possess moderate impedance matching and splendid attenuation constant as well as the optimal MA properties.

Conclusions

Summary, we have successfully synthesized Air@rGO€Co microspheres by a simple and efficient two-step method consisting of water-in-oil (W/O) emulsion technique and subsequent annealing process. The microspheres showed good electromagnetic properties because of the coexistence of magnetic loss and dielectric loss to microwaves. The minimum reflection loss (RL_{min}) value of $S_{1.5}$ reaches −68.1 dB at 13.8 GHz with a thickness of 2.2 mm, and the absorption bandwidth (lower than −10 dB) is 7.1 GHz covering from 10.9 GHz to 18.0 GHz. More interestingly, we can easily controll the microwave absorbing properties of the microspheres by changing the ratio of the two components in the composites. As the Co content increasing, the RL_{min} valve of Air@rGO€Co microspheres move to higher frequency rang. Our study provides a good potential method for preparation of lightweight microwave absorbing materials.

References

1. Wang, Z., Wu, L., Zhou, J., Shen, B. & Jiang, Z. Enhanced microwave absorption of Fe₃O₄ nanocrystals after heterogeneously growing with ZnO nanoshell. *Rsc Adv.* **3**, 3309–3315 (2013).
2. Hu, C. *et al*. 3D graphene-Fe₃O₄ nanocomposites with high-performance microwave absorption. *Phys. Chem. Chem. Phys.* **15**, 13038–13043 (2013).
3. Zhang, X. *et al*. Thermal conversion of an Fe₃O₄@metal-organic framework: a new method for an efficient Fe-Co/nanoporous carbon microwave absorbing material. *Nanoscale* **7**, 12932–12942 (2015).
4. Zhang, Y. *et al*. Broadband and tunable high-performance microwave absorption of an ultralight and highly compressible graphene foam. *Adv. Mater.* **27**, 2049–2053 (2015).
5. Lian, Q., Wang, L., Wu, H. & Wu, H. Effect of carbonization temperature on dielectric and microwave absorbing properties of cobalt doped mesoporous carbon composites. *Nano* **9**, 1450033 (2014).
6. Jian, X. *et al*. Facile Synthesis of Fe₃O₄/GCs Composites and Their Enhanced Microwave Absorption Properties. *Acs Appl. Materi. Interfaces* **8**, 6101–6109 (2016).
7. Qing, Y., Min, D., Zhou, Y., Luo, F. & Zhou, W. Graphene nanosheet- and flake carbonyl iron particle-filled epoxy-silicone composites as thin-thickness and wide-bandwidth microwave absorber. *Carbon* **86**, 98–107 (2015).
8. Liu, G. *et al*. One-pot synthesis of Ag@Fe₃O₄/reduced graphene oxide composite with excellent electromagnetic absorption properties. *Ceram. Int.* **41**, 4982–4988 (2015).
9. Wang, L., Huang, Y., Li, C., Chen, J. & Sun, X. Hierarchical composites of polyaniline nanorod arrays covalently-grafted on the surfaces of graphene@Fe₃O₄@C with high microwave absorption performance. *Compos. Sci. Technol.* **108**, 1–8 (2015).
10. Li, G. *et al*. Electromagnetic and microwave absorption properties of single-walled carbon nanotubes and CoFe₂O₄ nanocomposites. *Mater. Sci. Eng. B* **193**, 153–159 (2015).
11. Wang, H. *et al*. Cobalt/polypyrrole nanocomposites with controllable electromagnetic properties. *Nanoscale* **7**, 7189–7196 (2015).
12. Zong, M., Huang, Y., Zhang, N. & Wu, H. Influence of (RGO)/(ferrite) ratios and graphene reduction degree on microwave absorption properties of graphene composites. *J. Alloys. Compd.* **644**, 491–501 (2015).
13. Huang, Y., Wang, L. & Sun, X. Sandwich-structured graphene@Fe₃O₄@carbon nanocomposites with enhanced electromagnetic absorption properties. *Mater. Lett.* **144**, 26–29 (2015).
14. Fang, R. *et al*. Cyanate ester resin filled with graphene nanosheets and CoFe₂O₄-reduced graphene oxide nanohybrids as a microwave absorber. *Appl. Surf. Sci.* **351**, 40–47 (2015).
15. Pan, G., Zhu, J., Ma, S., Sun, G. & Yang, X. Enhancing the Electromagnetic Performance of Co through the Phase-Controlled Synthesis of Hexagonal and Cubic Co Nanocrystals Grown on Graphene. . *Acs Appl. Mater. Interfaces* **5**, 12716–12724 (2013).
16. White, S. R. *et al*. Autonomic healing of polymer composites. *Nature* **409**, 794–797 (2001).
17. Xiong, W. *et al*. A novel capsule-based self-recovery system with a chloride ion trigger. *Sci. Rep-UK.* **5**, 10866 (2015).
18. Wang, Y. *et al*. Self-immunity microcapsules for corrosion protection of steel bar in reinforced concrete. *Sci. Rep-UK.* **5**, 18484 (2015).
19. Cui, X. J. *et al*. Multi-stimuli responsive smart chitosan-based microcapsules for targeted drug delivery and triggered drug release. *Ultrason Sonochem.* **38**, 145–153 (2017).
20. Zhuo, R. F. *et al*. Multistep Synthesis, Growth Mechanism, Optical, and Microwave Absorption Properties of ZnO Dendritic Nanostructures. *J. Phys. Chem. C* **112**, 11767–11775 (2008).
21. Li, H. *et al*. Directed Growth and Microwave Absorption Property of Crossed ZnO Netlike Micro-/Nanostructures. *J. Phys. Chem. C* **114**, 10088–10091 (2010).
22. Ohlan, A., Singh, K., Chandra, A. & Dhawan, S. K. Microwave Absorption Behavior of Core−Shell Structured Poly (3,4-Ethylenedioxy Thiophene)−Barium Ferrite Nanocomposites. *Acs Appl. Mater. Interfaces* **2**, 927–933 (2010).
23. Lei, W. *et al*. Preparation, characterization and microwave absorbing properties of nano-sized yolk-in-shell Ni–P nanospheres. *J. Phys. D: Appl. Phys.* **48**, 355302 (2015).
24. Liu, Q. *et al*. CoNi@SiO₂@TiO₂ and CoNi@Air@TiO₂ Microspheres with Strong Wideband Microwave Absorption. *Adv. Mater.* **28**, 486–490 (2015).
25. Chen, Y. J. *et al*. Synthesis, Multi-Nonlinear Dielectric Resonance, and Excellent Electromagnetic Absorption Characteristics of Fe₃O₄/ZnO Core/Shell Nanorods. *J. Phys. Chem. C* **114**, 9239–9244 (2010).
26. Cao, J. *et al*. Large-Scale Synthesis and Microwave Absorption Enhancement of Actinomorphic Tubular ZnO/CoFe₂O₄ Nanocomposites. *J. Phys. Chem. B* **113**, 4642–4647 (2009).
27. Liu, J. *et al*. Microwave Absorption Enhancement of Multifunctional Composite Microspheres with Spinel Fe₃O₄ Cores and Anatase TiO2 Shells. *Small* **8**, 1214–1221 (2012).
28. Zeng, Q. *et al*. Air@rGO€Fe₃O₄ microspheres with spongy shells: self-assembly and microwave absorption performance. *J. Mater. Chem. C* **4**, 10518–10528 (2016).
29. He, H. & Gao, C. Supraparamagnetic, Conductive, and Processable Multifunctional Graphene Nanosheets Coated with High-Density Fe₃O₄ Nanoparticles. *Acs Appl. Mater. Interfaces* **2**, 3201–3210 (2010).
30. Si, Y. & Samulski, E. T. Exfoliated Graphene Separated by Platinum Nanoparticles. *Chem. Mater.* **20**, 6792–6797 (2008).
31. Zhao, B. *et al*. Corrosive synthesis and enhanced electromagnetic absorption properties of hollow porous Ni/SnO₂ hybrids. *Dalton Trans.* **44**, 15984–15993 (2015).

32. Zhao, B. *et al*. Synthesis of flower-like CuS hollow microspheres based on nanoflakes self-assembly and their microwave absorption properties. *J. Mater. Chem. A* **3**, 10345–10352 (2015).

33. Qi, X. *et al*. The synthesis and excellent electromagnetic radiation absorption properties of core/shell-structured Co/carbon nanotube-graphene nanocomposites. *Rsc Adv.* **6**, 11382–11387 (2016).

34. Lv, H. *et al*. Co$_x$Fe$_y$@C Composites with Tunable Atomic Ratios for Excellent Electromagnetic Absorption Properties. *Sci.Rep.* **5**, 18249 (2015).

35. Zhang, X. J. *et al*. Fabrication of multi-functional PVDF/RGO composites via a simple thermal reduction process and their enhanced electromagnetic wave absorption and dielectric properties. *Rsc Adv.* **4**, 19594–19601 (2014).

36. Tong, G. *et al*. Tunable dielectric properties and excellent microwave absorbing properties of elliptical Fe$_3$O$_4$ nanorings. *Appl. Phys. Lett.* **108**, 072905 (2016).

37. Meng, F. *et al*. Growth of Fe$_3$O$_4$ nanosheet arrays on graphene by a mussel-inspired polydopamine adhesive for remarkable enhancement in electromagnetic absorptions. *Rsc Adv.* **5**, 101121–101126 (2015).

38. Meng, Z., Ying, H. & Na, Z. Reduced graphene oxide-CoFe$_2$O$_4$ composite: Synthesis and electromagnetic absorption properties. *Appl Surf. Sci.* **345**, 272–278 (2015).

39. Ni, S. *et al*. Low temperature synthesis of Fe$_3$O$_4$ micro-spheres and its microwave absorption properties. *Mater. Chem. Phys.* **124**, 353–358 (2010).

40. Tong, G. *et al*. Synthesis and characterization of nanosized urchin-like α-Fe$_2$O$_3$ and Fe$_3$O$_4$: Microwave electromagnetic and absorbing properties. *J. Alloys. Compd.* **509**, 4320–4326 (2011).

41. Shi, X. L., Cao, M. S., Yuan, J. & Fang, X. Y. Dual nonlinear dielectric resonance and nesting microwave absorption peaks of hollow cobalt nanochains composites with negative permeability. *Appl. Phys. Lett.* **95**, 163108 (2009).

42. Lv, H. *et al*. Porous three-dimensional flower-like Co/CoO and Its excellent electromagnetic absorption properties. *ACS Appl. Mater. Interfaces* **7**, 9776–9783 (2015).

43. Lv, H., Ji, G., Liang, X., Zhang, H. & Du, Y. A novel rod-like MnO$_2$@Fe loading on graphene giving excellent electromagnetic absorption properties. *J. Mater. Chem. C* **3**, 5056–5064 (2015).

Acknowledgements

Author Contributions

Q.Z., P.C. and Q.Y. conceived the idea. Q.Z. carried out the materials synthesis. Q.Z., H.C., X.X., D.X. and Q.W. performed the materials characterization. Q.Z. and Q.Y. co-wrote the paper. P.C. together with other authors discussed and commented on the paper.

Additional Information

Supplementary information accompanies this paper at doi:10.1038/s41598-017-08293-3

Competing Interests: The authors declare that they have no competing interests.

Publisher's note: Springer Nature remains neutral with regard to jurisdictional claims in published maps and institutional affiliations.